JGR Atmospheres

RESEARCH ARTICLE
10.1029/2023JD039048

Australian Summer Monsoon Bursts: A Moist Static Energy Budget Perspective

Sarthak Mohanty[1,2], **Christian Jakob**[1,2], **and Martin S. Singh**[1,2]

[1]School of Earth, Atmosphere and Environment, Monash University, Melbourne, VIC, Australia, [2]ARC Centre of Excellence for Climate Extremes, Melbourne, VIC, Australia

Key Points:

- Australian monsoon burst moist static energy budget analysis reveals several distinct burst types
- Only one of the burst types follows the archetypal gross moist stability cycle of oceanic convection
- Horizontal moisture advection is critical for the burst evolution, but the details vary between types

Correspondence to:

S. Mohanty,
sarthak.mohanty@monash.edu

Citation:

Mohanty, S., Jakob, C., & Singh, M. S. (2024). Australian summer monsoon bursts: A moist static energy budget perspective. *Journal of Geophysical Research: Atmospheres*, *129*, e2023JD039048. https://doi.org/10.1029/2023JD039048

Received 11 APR 2023
Accepted 8 DEC 2023

Author Contributions:

Conceptualization: Sarthak Mohanty, Christian Jakob, Martin S. Singh
Data curation: Sarthak Mohanty
Formal analysis: Sarthak Mohanty
Funding acquisition: Sarthak Mohanty, Christian Jakob
Investigation: Sarthak Mohanty, Christian Jakob, Martin S. Singh
Methodology: Sarthak Mohanty, Christian Jakob, Martin S. Singh
Project Administration: Sarthak Mohanty, Christian Jakob
Resources: Sarthak Mohanty
Software: Sarthak Mohanty
Supervision: Sarthak Mohanty, Christian Jakob, Martin S. Singh
Validation: Sarthak Mohanty
Visualization: Sarthak Mohanty, Christian Jakob, Martin S. Singh
Writing – original draft: Sarthak Mohanty

Abstract The Australian monsoon's wet season is associated with sequences of wet and dry conditions known as bursts and breaks, which usually have timescales of a week or two. There are several hypotheses for the physical processes involved in monsoon bursts, ranging from the effects of the Madden-Julian Oscillation to extratropical influences. We analyze rainfall bursts in Northern Australia using a moist static energy (MSE) budget framework. We separate the bursts into three types and further separate them into pre-monsoon, active monsoon, and post-monsoon. We then apply ERA5 data to calculate the MSE budget for each burst and construct composite bursts for each of the three types. We find that the horizontal advection of MSE over the tropical northern Australian convergence zone is the most critical term in the budget for the day-to-day precipitation variation. MSE-related gross moist stability analysis reveals that each type has distinct characteristics. The burst type associated with active monsoon bursts displays convective growth and decay patterns both before and after the precipitation peak, which is typical of oceanic convection. A low-rainfall burst type, which is often seen before monsoon onset, is linked to coastal convection and has minimal rainfall decay after the burst. Finally, a sustained high-rainfall burst type, mostly observed at the end or after the monsoon retreat, has growth characteristics similar to the typical monsoon burst but does not decay, maintaining very high rainfall for at least a week due to a rearrangement of the circulation and local thermodynamic structure of the atmosphere.

Plain Language Summary The Australian Summer Monsoon (ASM) is associated with sequences of wet and dry conditions known as bursts and breaks during the extended summer months (October–April). Although understanding of these phenomena has progressed, there are still gaps in both our knowledge of the processes that produce bursts and our ability to predict their evolution. Energy budgets are evaluated in this study to gain insight into the key mechanisms involved in burst evolution. It is found that energy export/import via large-scale circulation is critical in determining the evolution of monsoon bursts. Furthermore, the research identifies various types of bursts, each with its own set of key mechanisms. These findings provide important insights into the dynamics of the ASM bursts and may help improve predictions of future bursts and breaks, allowing for better management of the region's agricultural and ecological systems.

1. Introduction

The Australian summer monsoon (ASM), which is a component of the Asia-Australia monsoon system, is responsible for a large portion of the precipitation in northern Australia during the extended summer months (November–April) (Krishnamurti & Chang, 1987; Nicholls et al., 1981; Wang, 2006). The arrival of the ASM is marked by a seasonal transition from dry south-easterly trade winds to moist north-westerlies over Northern Australia. This transition is associated with the global seasonal migration of the intertropical convergence zone, and it coincides with a transition between the equinoctial and solstitial Hadley Circulations (Gadgil, 2018).

The ASM is associated with sequences of wet and dry conditions known as bursts and breaks, which usually have timescales of a week or two (Drosdowsky, 1996; Moise et al., 2020; Pope et al., 2009). Bursts have a large impact on the natural environment, as well as regional effects on agriculture, infrastructure, and human settlements. Understanding their dynamics and consequences can help with regional planning and adaptation efforts (Adeloye & Rustum, 2011). Monsoon bursts can also produce extreme precipitation, thereby having implications for water management and flood prediction (Frei et al., 2000). The importance of bursts and breaks in the evolution of the ASM has been known at least since Troup (1961). Previous studies have associated intraseasonal variability in

Writing – review & editing: Sarthak Mohanty, Christian Jakob, Martin S. Singh

the monsoon to the Madden Julian Oscillation (Hendon & Liebmann, 1990), as well as, on shorter timescales, upper-level ridges and troughs originating in the subtropics (Keenan & Brody, 1988).

More recently, studies investigating the dynamics of ASM bursts have linked them to mid-latitude processes. For example, Berry and Reeder (2016) found that bursts were often initiated by the propagation of fronts across the continent, which themselves are linked to mid-latitude Rossby waves (see also Berry et al. (2012)). Narsey et al. (2017) used an analysis of the circulation budget over Northern Australia to corroborate and extend these results; they showed that bursts were associated with a rapid increase in cyclonic circulation, which could be triggered by approaching mid-latitude front-like features. They highlighted the influence of the mid-latitudes as a source of vorticity for burst circulations. Here, we take a complementary perspective, and we consider the sources of moisture and energy for bursts in the ASM.

A natural starting point in examining energy and moisture sources in the atmosphere is the column-integrated budgets of moisture q and dry static energy (DSE), s. However, in strongly precipitating regions, these budgets are dominated by large opposing terms corresponding to the heating and drying by moist convection on the one hand, and vertical advection by the circulation on the other hand. This makes analyzing causal mechanisms difficult since there is a close coupling between convective heating and vertical motion in the tropics.

An alternate approach is to analyze the column-integrated budget of the moist static energy (MSE), given by

$$h = s + L_v q, \tag{1}$$

where L_v, s, and q are the latent heat of vaporization, DSE, and specific humidity respectively. The MSE budget is used extensively in studying tropical dynamics (Chou et al., 2009; Neelin & Held, 1987), and as recently demonstrated by Inoue and Back (2017), it provides a framework for understanding the growth and decay of convective rainfall from an energy-based perspective.

The utility of the MSE budget arises as a result of three important properties of its budget. Firstly, MSE is approximately conserved under adiabatic displacement including condensation, and its column integral is therefore approximately unchanged under the effects of convection. Since MSE is equal to the sum of DSE and latent energy, convective heating effectively cancels with convective drying in the MSE budget, and changes in column-integrated MSE are instead related to the net energy input to the column by radiative and turbulent fluxes and transport of MSE by the circulation (Neelin & Held, 1987). A second important characteristic of the MSE budget is that, as a result of the weak horizontal temperature gradients that exist in the tropical atmosphere, temporal variations in MSE are almost entirely associated with moisture variations; variations in column-integrated MSE may therefore be interpreted as variations in column moisture content (Inoue & Back, 2017). Finally, it is well known that precipitation in the tropics is a very strong function of column water vapor (Bretherton et al., 2004). As such, variations in MSE may be statistically associated with variations in precipitation, and the MSE budget provides a link between energy input into the column and the growth and decay of precipitation anomalies (Inoue & Back, 2017).

Here, we apply the MSE budget to analyze the growth and decay of precipitation in bursts within the Australian monsoon. We examine how the net energetic forcing (including radiative and turbulent fluxes), and horizontal and vertical advection of MSE combine to govern the evolution of moisture and precipitation in the lead-up to and during monsoon bursts. Sekizawa et al. (2023) recently used a similar approach to show that an anomalous supply of MSE through horizontal advection plays an important role in maintaining interannual variability of the ASM. They find that anomalous westerlies to the northeast of the continent provide a source of MSE that sustains precipitation anomalies for up to a season. Here, we focus on the shorter, "synoptic," timescales of bursts, but we nonetheless find that horizontal advection plays a major role in governing their growth and decay, consistent with the results of Sekizawa et al. (2023).

A key diagnostic of the MSE budget is the gross moist stability (GMS). The GMS was introduced by Neelin and Held (1987) as a measure of the MSE stratification in a two-layer representation of the climatological circulation in the tropics. Raymond and Fuchs (2007) extended this concept by introducing the term normalized gross moist stability (NGMS), whose primary purpose is to represent the net export efficiency of some quantity conserved in a moist adiabatic process per unit of convection. In this study, we have taken the MSE as the conserved quantity and the net export of DSE as the unit of convection.

The NGMS is used for a variety of applications, one of which is to diagnose destabilization/stabilization mechanisms in ascending circulations (Benedict et al., 2014; Hannah & Maloney, 2011; Inoue & Back, 2015, 2017).

Large-scale ascent may destabilize the tropical atmosphere (negative GMS) if it is associated with a bottom-heavy ascent profile, with convergence in the MSE-rich boundary layer and divergence in the MSE-poor mid-troposphere. Stabilization of the atmosphere (positive GMS), on the other hand, is associated with a top-heavy ascent profile with MSE-poor lower tropospheric convergence and MSE-rich upper-tropospheric divergence.

On timescales relevant to bursts, the GMS can vary temporally and becomes difficult to define, but Inoue and Back (2015) have extended the destabilization/stabilization concept into shorter time scales by considering a phase space of dry-static energy divergence on one axis and moist-static energy divergence on the other which they refer to as the GMS plane. In this phase space, amplification and decay of precipitation anomalies are determined by whether the GMS on a given day is above or below a "critical" GMS that varies on slower timescales. The authors go on to show that oceanic precipitation variability is characterized by a life cycle in the GMS plane (Inoue & Back, 2017), and that horizontal advection of MSE is a key process driving ubiquitous precipitation variability over the oceans (Inoue et al., 2021).

We use the above GMS-plane concept in this study to investigate the mechanisms of amplification and decay of bursts in the ASM. Consistent with previous work over the ocean (Inoue et al., 2021) and in the ASM on seasonal timescales (Sekizawa et al., 2023), we find horizontal MSE advection to be the major control on the evolution of bursts. However, some bursts can have a substantially different life cycle in the phase space compared to precipitation variability over the ocean, and this leads us to a novel categorization of ASM bursts based on their path through the GMS plane. Our results provide a new perspective on bursts focused on the moisture and energy budgets that is complementary to previous studies that have highlighted the dynamics of vorticity.

The paper is structured as follows. In Section 2 we present our methodology and data set selection, followed by the results in Section 3. The findings are divided into three sub-sections: Section 3.1 discusses the Monsoon Burst Composite Characteristics, Section 3.2 presents the composite monsoon burst's MSE Budget, and Section 3.3 discusses a novel monsoon burst classification in the GMS-plane. Section 4 provides a summary and our main conclusions.

2. Data and Methodology

As the goal of this study is to combine the rainfall evolution of Australian monsoon bursts with the evolution of MSE and its budget, we use rainfall, radiative fluxes, and turbulent surface fluxes as well as upper-level data obtained from the European Center for Medium-Range Weather Forecasts fifth generation reanalysis (ERA5) with a horizontal grid spacing of $0.25° \times 0.25°$ and with 37 vertical pressure levels.

We calculate all budget terms hourly and then average them daily. We note that the ERA5 rainfall and flux data are a model output rather than an observation, but we prefer to use them to achieve a better budget closure. Using alternative data sources for rainfall, such as the Global Precipitation Climatology Project (GPCP) data set (Adler et al., 2022), does result in small quantitative differences, but does not affect the overall main conclusions of this study. We have also repeated all analyses using the NASA MERRA-2 reanalysis (Gelaro et al., 2017). Once again we find that while some quantitative differences exist between the different reanalysis, our main conclusions remain unaffected. All analyses are performed for a box centered on the ASM region ranging from 11°S to 18°S and 125°E to 145°E (see Figure 2a) for the years 1997–2020. Using this subset of the ERA5 data constitutes a compromise in creating a large enough sample of bursts whilst balancing the significant computational costs of the MSE budget analysis, whilst also ensuring the best observational coverage in the ERA5 period.

The first step in our analysis is the definition of monsoon bursts from the daily rainfall time series. Here we follow the methodology of Berry and Reeder (2016) and Narsey et al. (2017) to define the bursts, which is illustrated in Figure 1. First, we calculate a daily time series by averaging the rainfall over northern Australia for the extended summer months (October–April) from 1997 to 2020. We then define a smoothed seasonal climatology by taking the mean over all years and applying a low pass filter (Fourier transform retaining the first six harmonics; blue dashed line on Figure 1). We also construct a smoothed standard deviation by applying the same low-pass filter to the seasonal climatological standard deviation.

The smoothed seasonal climatological mean, plus and minus half a smoothed standard deviation, defines the limits of high and low rainfall (red and green lines on Figure 1). We then overlay an individual monsoon season's rainfall time series with the smoothed mean and standard deviations (Figure 1b). A burst is defined as a rise in

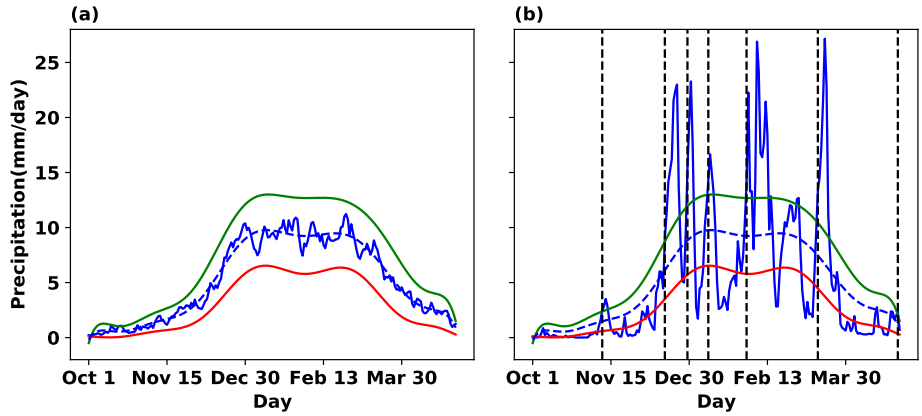

Figure 1. (a) Climatological seasonal cycle of precipitation over the Northern Australia region (blue solid), smoothed climatology (blue-dashed), and smoothed climatology plus (green) and minus (red) 0.5 smoothed standard deviations defining the high and low precipitation limits. (b) As in (a) but with precipitation for 2003–2004 instead of the climatological mean. Days of burst initiation are marked on (b) with vertical dashed lines.

daily precipitation from below the low precipitation limit to above the high precipitation limit over a period of no more than 7 days. A burst lasts until the rainfall falls below the lower precipitation limit again. The seven bursts identified by this method for the example year shown in Figure 1b are highlighted by vertical lines. Using this method we identify a total of 125 bursts.

As our goal is to link the evolution of the rainfall bursts with the MSE budget, we calculate all budget terms for a 15-day period ranging from 7 days before to 7 days after the start day of each burst. While in principle, a single day can contribute to more than one burst, we find only two overlapping bursts with a maximum of 2 days overlap between them.

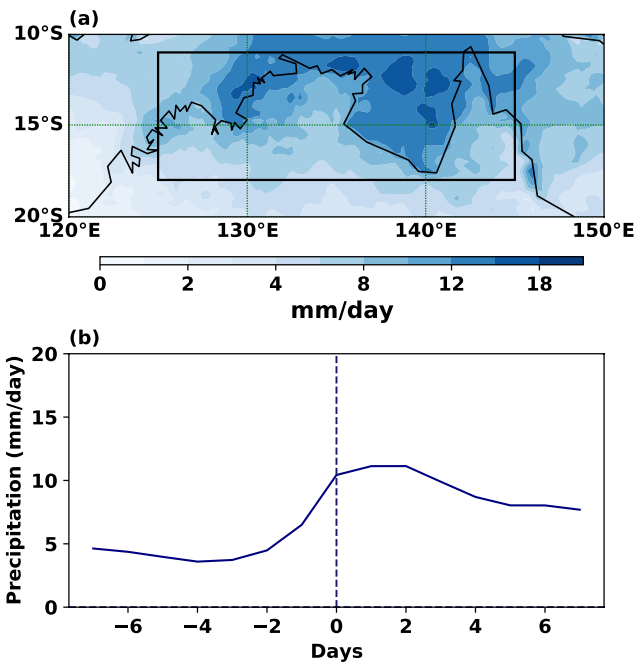

Figure 2. (a) Composite precipitation for "day 0" of monsoon bursts (b) Composite precipitation temporal evolution for all bursts averaged over box shown in (a).

The column-integrated Moist Static Energy; MSE (Hill et al., 2017, 2018; Neelin & Held, 1987) budget equation for a single location can be expressed approximately as follows:

$$\frac{\partial\{h\}}{\partial t} + \nabla\cdot\left\{h\vec{v}_h\right\} = L_v E + H + R_t + R_s, \tag{2}$$

where MSE is defined as $h = c_p T + gz + L_v q$. c_p is the specific heat capacity at constant pressure, T is the temperature, g is the gravitational acceleration, z is height and q is specific humidity respectively. $L_v E$, H, R_t, and R_s are latent heat flux (LHF), sensible heat flux (SHF), and net radiation at the top of the atmosphere and the surface respectively. The curly brackets denote the column mass integral defined $\{\cdot\} = \int_0^{p_s}(\cdot)dp/g$, where p_s is the surface pressure.

We calculate the divergence term by applying the divergence theorem to integrate the fluxes along the boundary of our analysis area. In doing so we apply a correction to the boundary velocities to ensure mass conservation (see Appendix A for more detail). We find that the mass constraint improves the closure of the MSE budget.

An important quantity in our analysis is the gross moist stability (GMS), as it provides a measure to connect circulation and convection. We adopt the definition of GMS by Raymond et al. (2009), as

$$GMS = \frac{\nabla\cdot\left\{h\vec{v}_h\right\}}{\nabla\cdot\left\{s\vec{v}_h\right\}} \approx \frac{\left\{\omega\frac{\partial h}{\partial p}\right\}}{\nabla\cdot\left\{s\vec{v}_h\right\}} + \frac{\left\{\vec{v}_h\cdot\nabla h\right\}}{\nabla\cdot\left\{s\vec{v}_h\right\}} \tag{3}$$

As before, $\nabla \cdot \left\{h\vec{v}_h\right\}$ is the net divergence of MSE, while $\nabla \cdot \left\{s\vec{v}_h\right\}$ denotes the net divergence of dry static energy (DSE), which is defined as $s = c_p T + gz$. Further, ω is the vertical pressure velocity. In Equation 3 we decompose the overall divergence of MSE into its vertical advection ($\{\omega\partial_p h\}$) and horizontal advection $\left(\left\{\vec{v}_h \cdot \nabla h\right\}\right)$ components. Inoue and Back (2015) have shown that convectively active days are characterized by a positive DSE flux divergence, that is $\nabla \cdot \left\{s\vec{v}_h\right\} \geq 0$.

Inoue and Back (2015) introduce another useful GMS-related quantity, called the Drying Efficiency (DEF), which can be used to identify growth and decay phases in convection. The DEF can be computed by calculating GMS (τ) and a critical GMS (τ_c) and taking their difference. The critical GMS is defined as:

$$\tau_c = \frac{L_v E + H + R_t + R_s}{\nabla \cdot \left\{s\vec{v}_h\right\}} = \frac{NEF}{\nabla \cdot \left\{s\vec{v}_h\right\}}, \tag{4}$$

where *NEF* denotes the net energetic forcing on the analysis area. This leads to the definition of the *DEF* as:

$$DEF = \tau - \tau_c = \frac{\nabla \cdot \left\{h\vec{v}_h\right\} - NEF}{\nabla \cdot \left\{s\vec{v}_h\right\}} \tag{5}$$

Neglecting the column DSE tendency ($\partial_t\{s\}$) by making use of the commonly applied weak temperature gradient (WTG) assumption (Sobel et al., 2001) which assumes that the temporal as well as spatial variations of temperature are much smaller than the variations in moisture we can apply Equation 2 to yield approximately:

$$DEF \approx \frac{-\partial\{L_v q\}/\partial t}{\nabla \cdot \left\{s\vec{v}_h\right\}}, \tag{6}$$

According to Equations 5 and 6, for a convectively active day $\left(\nabla \cdot \left\{s\vec{v}_h\right\} \geq 0\right)$ we find that for $\tau - \tau_c > 0$ water vapor in the column will decrease ($\partial\{L_v q\} < 0$) indicating a decaying phase of convection. Equally, for $\tau - \tau_c < 0$ we find ($\partial\{L_v q\} > 0$), indicating a moistening of the column and an associated increase in rainfall.

Below, we apply the MSE-budget analysis to all ASM bursts identified in the ERA5 record. However, we also recognize that the characteristics of the bursts may vary significantly from burst to burst and throughout different stages of the monsoon season. We investigate this in two ways. First, we perform a cluster analysis on the bursts, using the temporal evolution of the numerator and denominator of the GMS definition as inputs to the clustering algorithm (Equation 3, see Section 3.3 for more details). We use the k-means clustering algorithm (Lloyd, 1982), which is widely used in pattern recognition (Baraldi & Blonda, 1999) and clustering (Gentleman & Carey, 2008) based on a centroid method. The k-means cluster divides a set of "N" samples into K distinct clusters by locating the K cluster centers (or centroids) in such a way that the sample assigned to a centroid is closer to it than to any other. Specifically, we apply the Python (sklearn) package using the k-means option to calculate our clusters.

To address the potential variation of bursts through the different stages of the ASM, we classify each burst as pre-monsoon, monsoon, or post-monsoon. This classification is accomplished by specifying simple onset and retreat criteria. We note that there are many different definitions of monsoon onset and retreat for the ASM, many of which use local criteria at individual stations (Davidson et al., 2007; Evans et al., 2012, 2014; Kajikawa et al., 2010; Troup, 1961). As our analysis area is quite large, we apply a simple yet effective definition for the whole area. Monsoon onset occurs when the north-westerly trade winds persist over the northern boundary of our study region for at least 2 days, and the area-averaged precipitation minus evaporation is greater than zero for the first time in the ASM season (ONDJFMA). The retreat is defined as the first time after onset in the season when the region's average precipitation minus evaporation is less than zero with the presence of south-easterly trade winds for at least 2 days. We note that from hereon the term monsoon burst refers to all bursts during the overall wet season, including pre-, post- and active monsoon bursts. This expanded perspective is crucial because these bursts make substantial contributions to the total precipitation during their respective seasons.

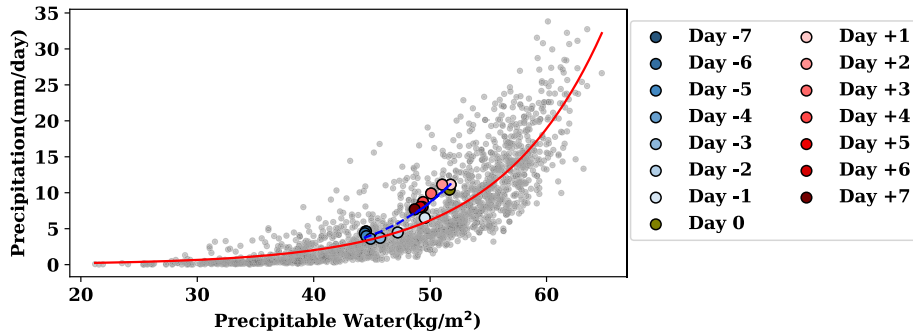

Figure 3. Scatter plot of precipitable water versus precipitation for all bursts (gray dots), overlain with the burst composite from 7 days before to 7 days after the burst.

3. Results

3.1. Monsoon Burst Composite Characteristics

We begin our analysis by investigating some basic characteristics of the monsoon bursts (see Section 2 for their definition) by averaging over all bursts to form a composite burst. Figure 2a shows the spatial pattern of precipitation on "day 0" (the day when the precipitation has crossed the higher precipitation limit) of the composite burst over the northern Australian region including our analysis area denoted by the rectangular box. It is evident that the ocean receives more precipitation compared to land, although the Northern Territory and northern Queensland are also significantly affected by the precipitation burst. The time-evolution of the area-averaged precipitation for the composite of bursts is shown in Figure 2b. Precipitation is nearly constant or has a slightly decreasing trend from seven to 3 days before the burst. It then begins to increase up to "Day 0," where it shows a slightly increasing trend until 2 days later when it begins to decrease.

Before linking the temporal evolution of burst rainfall with the MSE budget and GMS, we compare the burst composite precipitation amount with the precipitable water in the atmosphere. It is well-known from several previous studies (Bretherton et al., 2004; Holloway & Neelin, 2009), that there is an exponential relationship between these two variables in the tropics. We find that such a relationship holds for all burst days (Figure 3), albeit with significant scatter around the best fit line. An exponential relationship also holds across the time evolution of the composite burst (Figure 3). The composite relationship consistently lies above the best fit line for all burst days. This is the result of notable rainfall amount variability across bursts and will be explored further in Section 3.3. In the composite Days −7 to −3 are characterized by low precipitation accompanied by low precipitable water. The increase in precipitation from days −2 to +1 is accompanied by an increase in precipitable water followed by a decrease in both. We will exploit the relationship between the change in precipitation and the change in water vapor ($\partial_t P \propto \partial_t\{L_v q\}$) in the MSE budget analysis below.

3.2. The MSE Budget of the Composite Monsoon Burst

3.2.1. Time Evolution of the MSE Budget

To investigate different influences on precipitation evolution during rainfall bursts, we calculate the MSE budget for each burst.

In addition to the complete MSE budget, we also apply the tropical WTG approximation ($\partial_t\{s\} \approx 0$), which allows us to rewrite Equation 2 as:

$$\frac{\partial\{Lq\}}{\partial t} \approx -\nabla \cdot \left\{h\vec{v}_h\right\} + L_v E + H + R_t + R_s \tag{7}$$

Each term of Equation 2 is computed for each burst and averaged to form the burst composite as before. Figure 4 shows the composite time evolution of all budget terms along with that of the vertically integrated specific humidity ($\partial_t\{Lq\}$). Figure 4b shows the decomposition of the NEF into its individual components of the latent heat flux (LHF, dashed olive), sensible heat flux (SHF, dotted dashed olive) and net radiative heating of the atmosphere (dotted dashed black). We also show the difference of the left- and right-hand side of Equation 2 (purple dashed

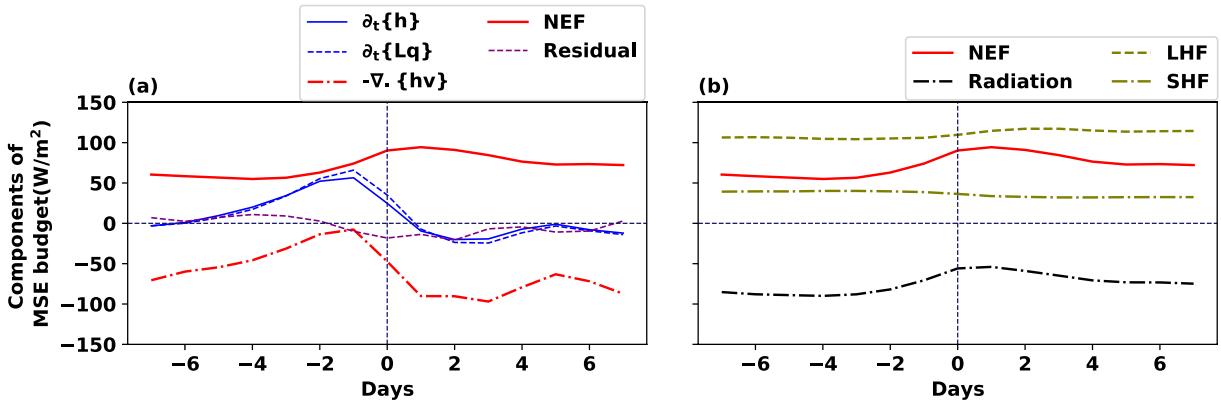

Figure 4. (a) Components of moist static energy budget in the burst composite (b) Detailed decomposition of net energetic forcing with latent heat flux, sensible heat flux, and net radiative heating.

line) showing a good closure of the budget in the burst composite throughout the burst evolution. We note that the mass-correction to the wind fields applied in our analysis significantly improved this closure (not shown). It is evident that the time evolution of the rate of change of MSE (solid blue line in Figure 4a) is nearly identical to that of vertically integrated humidity (dashed blue line), justifying the assumption made in Equation 7. Visually, it is also evident that the time evolution of the storage terms is closely related to the convergence of MSE (dot-dashed red line), while the NEF (solid red line) time evolution is different from that of those two terms. A quantitative calculation using the relative weight analysis technique (Tonidandel & LeBreton, 2011) confirms this result with the MSE convergence and NEF contributing 93% and 7%, respectively, to the overall temporal variation of the MSE and moisture tendency. This signifies the dominance of the circulation over local thermodynamic processes in the above temporal variation.

Seven days before the burst, the generation of MSE by local processes is roughly balanced by its divergence. For the next 7 days the divergence of MSE steadily decreases with only small changes in the NEF, leading to an accumulation of MSE, synonymous with an accumulation of moisture, in the analysis domain. As the rainfall begins to increase at about Day-2, the positive MSE (moisture) tendency levels off and it becomes negative at Day+1, the peak of the rainfall burst. Accompanying the rainfall increase is an increase in the NEF. As is evident in Figure 4b, this is to first order the result of a decrease in the radiative cooling, likely owing to increases in high-level clouds associated with the rainfall increases (Slingo & Slingo, 1988). A small increase in the LHF and a decrease in the SHF after the main rainfall event can also be seen, consistent with a wetter land surface.

3.2.2. Monsoon Burst GMS and Drying Efficiency Evolution

Having characterized the overall time evolution of the MSE budget for the composite monsoon burst, we now analyze how it is related to the evolution of the GMS and its components. In particular, we apply the concepts of the GMS plane and DEF developed by Inoue and Back (2015) to the monsoon burst evolution. As discussed in Section 2 the net divergence of MSE and DSE averaged over the northern Australian box are used to define the GMS (Equation 3). Both are calculated for each burst and averaged to describe the composite burst behavior as before.

Instead of calculating the ratio of these two quantities to yield GMS values we follow Inoue and Back (2015) and show them in a 2D-plane (Figure 5a). Each colored dot represents a day within the composite burst life cycle. The shaded ellipse around each dot represents the standard deviation of MSE and DSE divergence, respectively. It is evident, that the composite bursts follow a nearly closed loop in this diagram. Days −7 to −3 are characterized by relatively low values of DSE divergence (low convective activity). At the same time, there is a steady decrease in the divergence of MSE (see also Figure 4). Day −2 and −1 are characterized by a rapid increase in the divergence of DSE (convective activity) while the divergence of MSE remains low. Day 0 and +1, the days of the largest rainfall rates in the burst composite show the largest DSE divergence as expected with an increase in MSE divergence on Day+1. Days +2 to +7 show a steady reduction in both DSE and MSE divergence, almost, but not entirely, returning the system to the state at the start of the bursts at Day-7.

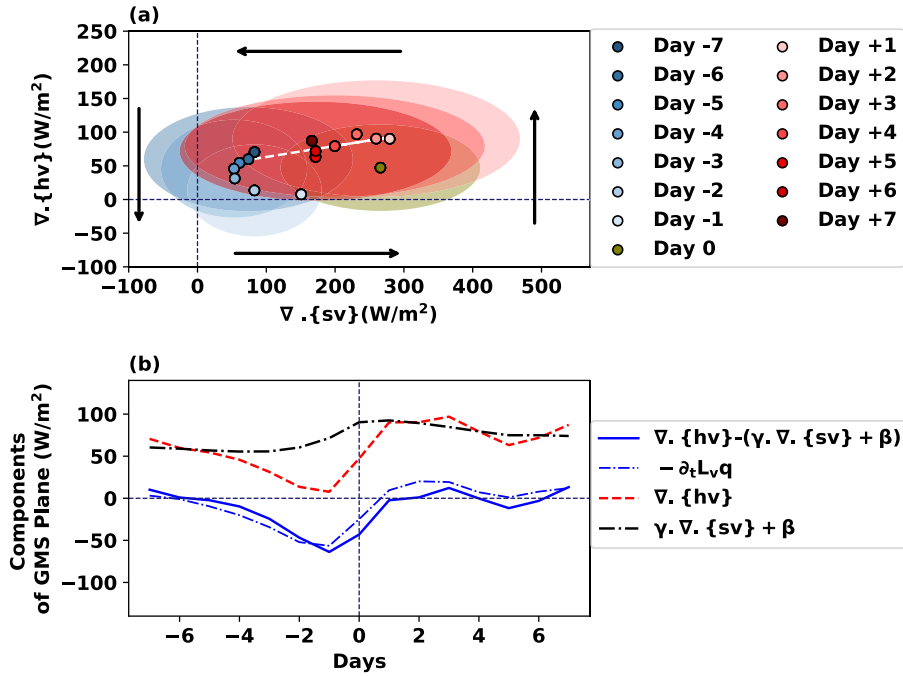

Figure 5. (a) Scatter plot of moist static energy divergence against dry static energy divergence for the composite of all bursts, with the NEF as the trend-line with slope. (b) Time evolution of key gross moist stability characteristics.

Inoue and Back (2015) and Inoue and Back (2017) suggest that the GMS plane can be applied to identify the life cycle of tropical convection. They show that the evolution of the net energetic forcing in the MSE life cycle can be linearly related to the DSE divergence as

$$NEF \approx \gamma \nabla \cdot \left\{ s\vec{v}_h \right\} + \beta. \tag{8}$$

We calculate the parameters of this relationship using the least-square fit of the NEF and DSE divergence and show the resulting linear relationship in Figure 5a. By applying the concept of the DEF (Inoue & Back, 2017) expressed in Equations 5 and 6, we can expect that points falling below the regression line indicate a growth phase of convection, while points above this line are indicative of decaying convective activity. The growth phase of the composite monsoon burst (Days −4 to 0) follows this expectation well. However, the decay phase of the bursts does not meet the expectation of a "simple" convective life cycle, with the days after the rainfall maximum all close to the regression line, rather than well above it. We will investigate this unexpected behavior further in Section 3.3.

An alternative way of investigating the convective life cycle of the bursts is to evaluate the time evolution of the DEF and its component terms (Equations 5 and 6). The numerators of the two equations $\left(\nabla \cdot \left\{ h\vec{v}_h \right\} - \left(\gamma \nabla \cdot \left\{ s\vec{v}_h \right\} + \beta \right)\right)$ and $-\partial_t \{L_v q\}$ are shown as solid and dot-dashed blue lines in Figure 5b. Once again we see the dominance of the moisture evolution in the evolution of the MSE budget. Consistent with the above discussion, negative values of the DEF indicate a growth phase of convection, while positive values are associated with a decay of convection (Inoue & Back, 2017). As $\nabla \cdot \left\{ s\vec{v}_h \right\}$ is positive throughout the burst, the signs of the two blue lines in Figure 5b are indicative of the life-cycle phase. As expected, we find a clear growth phase before the burst peak, with a much weaker signal in the decay of the convection after the burst peak. Consistent with our MSE budget discussion above, the temporal evolution of the DEF is closely related to the MSE divergence (red) with only a small influence from the energetic forcing (black).

3.2.3. Horizontal and Vertical Components of MSE Divergence

Several previous studies (Inoue et al., 2021; Sekizawa et al., 2023) have suggested that the horizontal advection of MSE, and in particular that of moisture, play a key role in the evolution of convective systems in the tropics. We investigate whether this holds for the ASM rainfall bursts by decomposing the MSE divergence

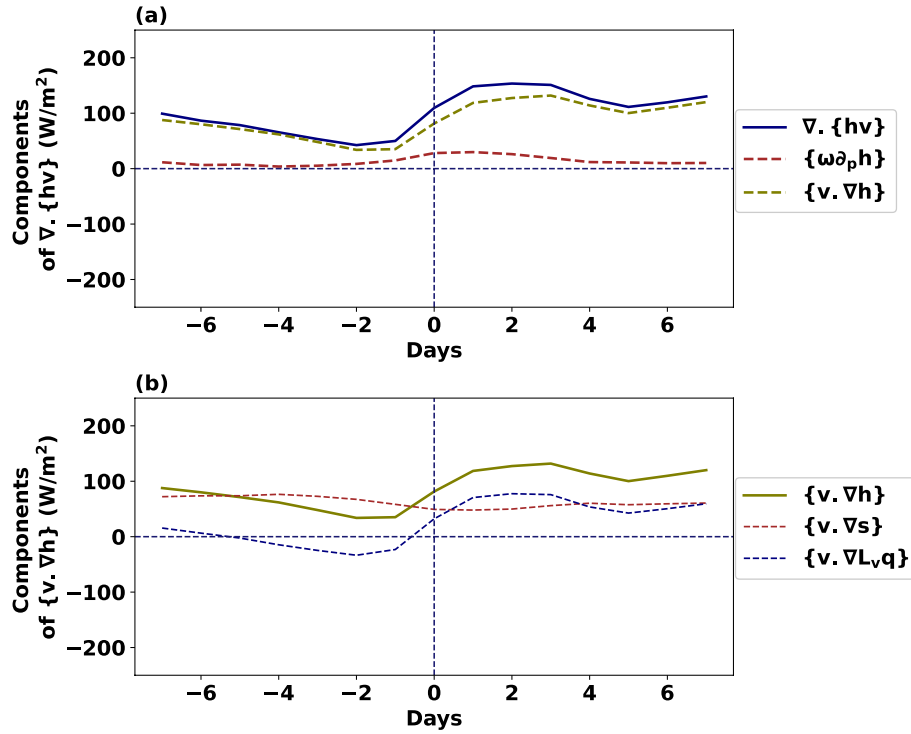

Figure 6. (a) Decomposition of moist static energy (MSE) divergence into its vertical and horizontal advection components. (b) Decomposition of the horizontal advection of MSE into its dry static energy and moisture components.

into contributions from horizontal and vertical advection making use of the continuity equation in pressure coordinates:

$$\nabla\{\cdot h\vec{v}_h\} = \{\vec{v}_h \cdot \nabla h\} + \left\{\omega\frac{\partial h}{\partial p}\right\} \tag{9}$$

As the advection terms on the right hand side of Equation 9 cannot be calculated simply by their boundary values, we cannot apply the mass budget corrections we used so far in calculating the full divergence terms. Hence, we use the uncorrected winds to calculate the two advection terms. Once again, the decomposition is applied to all bursts individually and averaged to produce the composite shown in Figure 6a. MSE divergence, as well as horizontal and vertical advection, are indicated by thick blue lines, dashed olive lines, and red lines, respectively. We note that as expected, the net divergence obtained by adding the two advection terms (blue line) differs in magnitude from that obtained using the mass-corrected boundary velocities (dashed red line in Figure 5b). However, the temporal evolution throughout the burst is nearly identical. As it is this evolution we are aiming to understand, the use of the uncorrected values when decomposing divergence terms into advection components is therefore justified.

It is evident that the horizontal advection of MSE closely follows the time evolution of the total divergence of MSE whereas the vertical advection is close to zero throughout with a small peak around Days 0 and 1. The reason for the small contribution from vertical advection is that its moisture ($\{\omega\partial_p Lq\}$) and DSE contributions ($\{\omega\partial_p s\}$) are of near equal magnitude and opposite sign, implying a small value of GMS (not shown). This is not true for the horizontal components (Figure 6b). Here, MSE, DSE, and moisture horizontal advection are denoted by thick olive, dashed red, and dashed blue lines, respectively. We find that the horizontal DSE advection makes a near-constant in time contribution to the horizontal MSE advection, which is dominated by the temperature term in the DSE (not shown). This indicates that horizontal temperature gradients do in fact exist and make a constant (in time) contribution to the budget. Nevertheless, as was shown in Figure 4, the time derivative of DSE for the region is close to zero, indicating a balance between horizontal and vertical advection of DSE and the local forcing terms. In contrast to the time-invariant horizontal advection of DSE, the time evolution of the horizontal advection of moisture in the burst composite closely follows that

of the horizontal advection of MSE, highlighting its dominant role in shaping this evolution. Noting the sign convention, moisture is advected into the box a few days before the burst onset and out of the box in the active phase of the burst. This is consistent with both the evolution of the rainfall and box-average humidity discussed above.

3.3. Monsoon Burst Classification in the GMS-Plane

The above analysis of monsoon bursts has shown that the temporal evolution of the composite burst MSE budget closely resembles that of convective events observed over the tropical oceans found in earlier studies (McBride & Frank, 1999; Pope et al., 2008). However, Figure 5a also indicates that there is a very large variation between individual bursts as expressed by very large standard deviations in the GMS plane analysis. This implies that the different characteristics of the individual bursts may be compensated for each other in the composite, resulting in the loss of differences in the processes associated with potentially different types of bursts. We investigate the existence of different classes of bursts by applying a cluster analysis to the two quantities spanning the GMS plane ($\nabla \cdot \{h\vec{v}_h\}$ and $\nabla \cdot \{s\vec{v}_h\}$). The two variables for each day for each burst form the (30-element) input vectors to a k-means cluster analysis (detailed in Section 2).

After some experimentation and using a mixture of subjective and objective criteria suggested by Rossow et al. (2005), we find that three clusters (named C1, C2, and C3) best separate the different types of rainfall bursts. Using fewer clusters misses important differences, while additional clusters only provide a very small further separation of the three key types of bursts described below.

Figure 7 summarizes the main results of the cluster analysis by presenting the rainfall evolution (Figure 7a–7c), the evolution of the bursts on the GMS plane (Figure 7d–7f) and the components of the DEF as well as the evolution of the horizontal moisture advection (Figure 7g–7i).

The rainfall evolution of the bursts clearly distinguishes the three clusters. C1, which contains 31% of all bursts, most closely resembles the overall composite (compare Figure 7a with Figure 2b), with the important difference that the rainfall returns to the pre-burst values, while it remains above them in the overall composites. This difference results from the rainfall evolution in C2 (37% of all bursts) and C3 (32% of all bursts). In both cases, rainfall remains steady after the onset of the burst, with C2 showing very low rainfall values, while C3 is characterized by maintaining high rainfall all the way from Day 0 to Day+7.

The three clusters are also distinct in when the bursts they represent occur during the monsoon season. While all types can occur in all parts of the season, C1 is most common during the active monsoon (61% of its cases). In contrast, almost all of the cases in C2 occur during the pre-monsoon or post-monsoon seasons when the south-easterly trade winds dominate. In general, C2 is characterized by weak precipitation bursts that occur outside of the monsoon season. When we calculate C2's contribution to total precipitation accumulated across all clusters, we see that it only accounts for 11.5%. We included C2 bursts in this study because they are still important as a water source and contribute significant precipitation during the low rainfall seasons during ASM. C3 bursts occur mostly during the monsoon and post-monsoon (late February-early March).

Figure 7d–7f show the evolution of the three burst types in the GMS plane. C1 closely resembles the life-cycle of convection identified by earlier studies for convection over the tropical oceans (Inoue & Back, 2017; Inoue et al., 2021). The pre-burst days can be found in the area indicating the growth of convection (below the line defined by the NEF). The days following the maximum of rainfall on Day+1, can be found in the convective decay region (above the NEF line). Furthermore, Day+7 is found close to Day-7 indicating a return of the monsoon region to its state at the start of the burst.

In contrast, in C2 the majority of days before Day 0 show negative values of DSE divergence $\left(\nabla \cdot \{s\vec{v}_h\} < 0\right)$, which indicate convectively inactive periods (Inoue & Back, 2015). Only Day-1 and Day 0 fall into the convective growth region of the diagram with the days following the burst showing little sign of convective decay. These findings are consistent with the occurrence of C2 bursts predominantly during the pre-and post-monsoon periods respectively.

The growth of convection in the bursts in C3 closely resembles that of C1 and the overall burst composite. However, as expected from the rainfall evolution for this burst type, there is no convective decay phase after the burst onset. Instead, Days +1 to +7 remain near but below the NEF line, consistent with continuing high rainfall

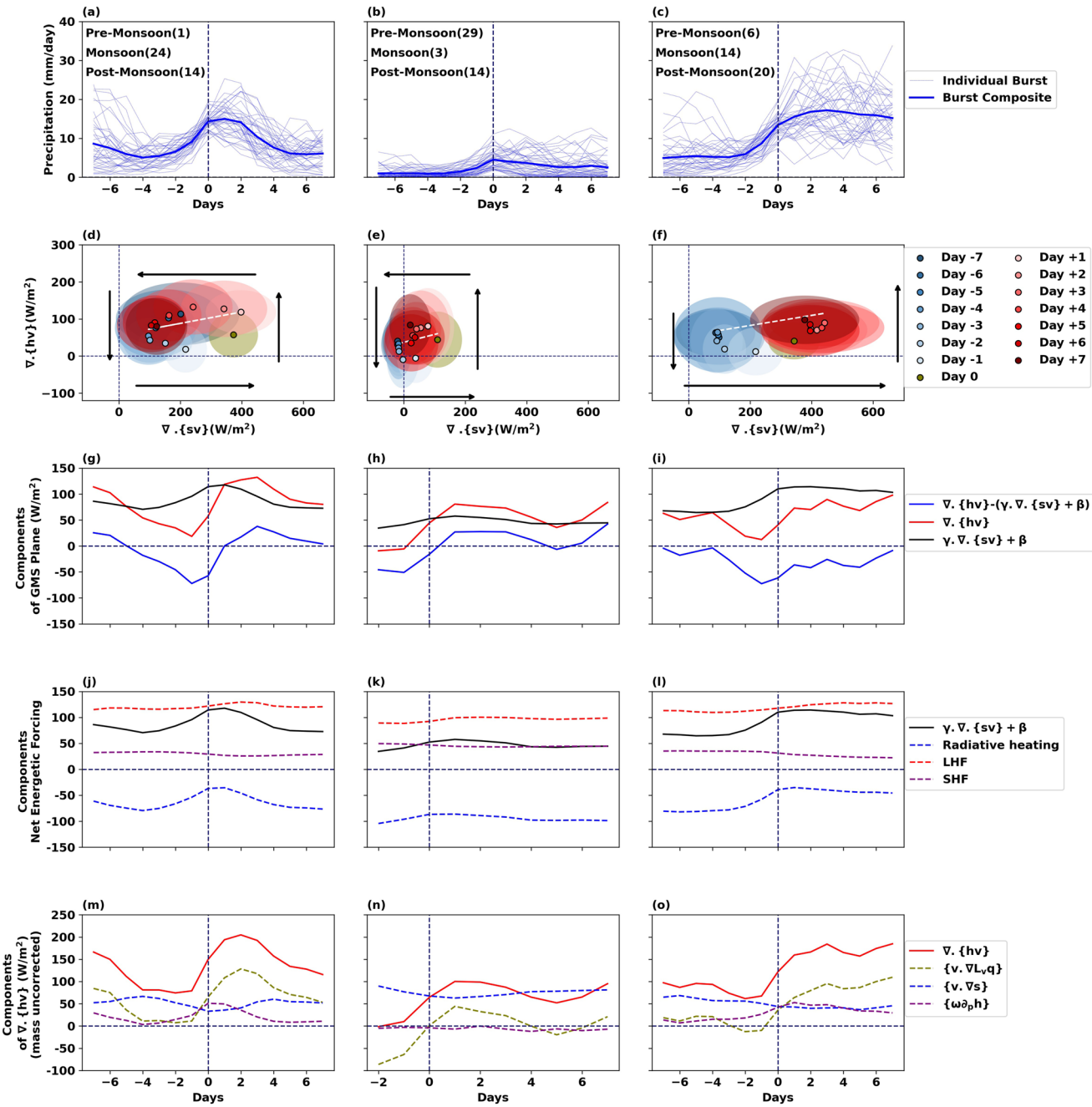

Figure 7. Composite behavior of the three rainfall burst types (see text): Temporal evolution of precipitation (a)–(c), GMS-plane composites (d)–(f), the temporal evolution of the drying efficiency components (g)–(i), the temporal evolution of the net energetic forcing (j)–(l), the temporal evolution of the components of the moist static energy divergence (mass-uncorrected) (m)–(o).

values throughout that period. Extending the analysis of the bursts beyond Day+7 shows that the burst decay does occur, but only from Day+8 onward (not shown).

Figures 7g–7i shows the time evolution of the key components of the DEF together with the horizontal moisture advection for the three clusters. As Day −7 to Day −4 are convectively inactive in C2 we only considered the days following Day −3. The bursts of C1 show an amplifying phase of convection (DEF less than 0) from Day −5 to Day 0. This is accompanied by a reduction in the export of MSE (red line) associated with a reduction in the drying by moisture advection. This allows a net accumulation of MSE and moisture through local thermodynamic processes creating the conditions for the burst to occur. From about Day +1, the export of MSE, associated with

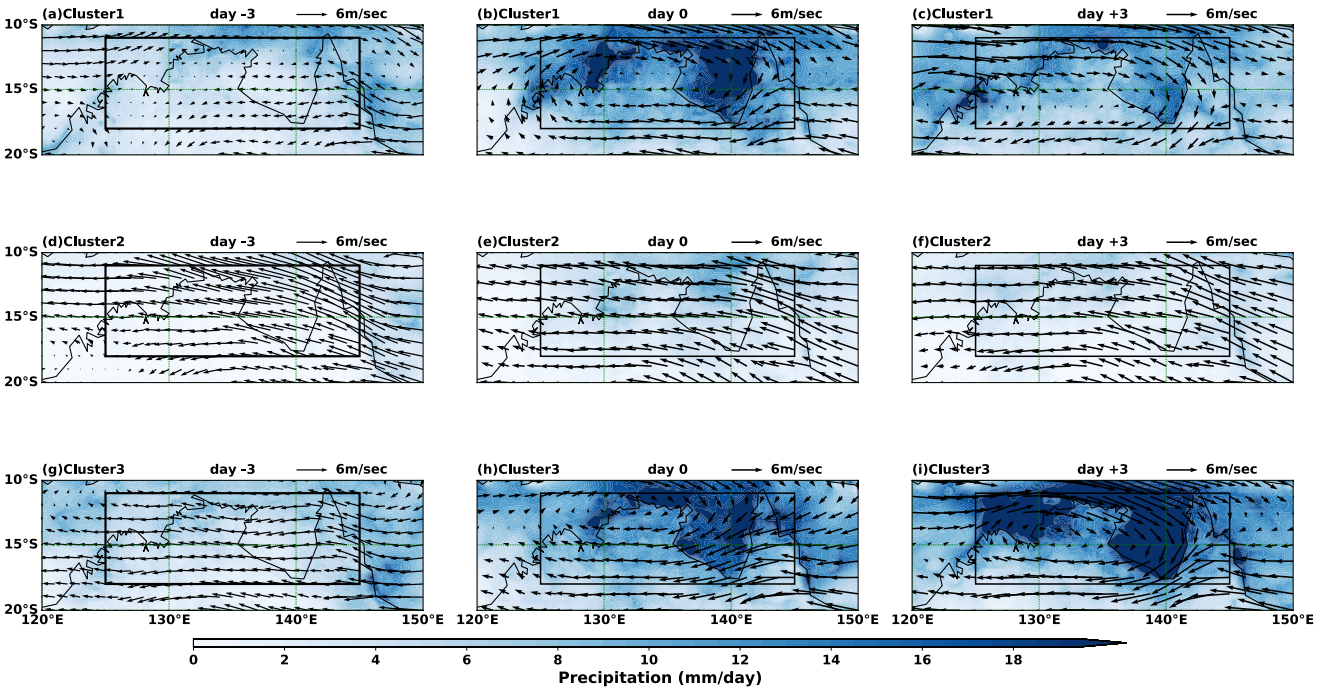

Figure 8. Mean precipitation and 850hpa wind for Day-3 (left), Day 0 (middle) and Day+3 (right) for C1 (top), C2 (middle) and C3 (bottom).

drying by moisture advection, exceeds the effects of the local processes, leading to the decay phase of convection. This evolution, once again, most strongly matches that reported for convection over the tropical oceans (Inoue & Back, 2017).

The growth phase of the bursts in C3 resembles that of C1 with an amplification of convection evident from Day −4. A notable difference in this phase is the role of moisture advection. While C1 shows a reduction in the drying of the analysis region, moisture advection in C3 remains close to zero throughout the entire pre-burst period. Only after the burst does the drying through moisture advection dominate the MSE export. Unlike C1, instead of decaying after reaching the burst peak the DEF indicates a potential for a further growth of convection. This is related to an increase in the net energetic forcing after the burst brought about by a combination of a reduction in radiative cooling and an increase in the LHF (most likely due to wetter soil conditions at the end of the monsoon). In contrast, the export of MSE only slowly increases, reaching values of similar magnitude to the local forcing only at Day+7. Consistent with this evolution, precipitation remains nearly constant, making C3 the strongest burst cluster.

In the bursts of C2, convective amplification only begins 2 days before the burst. Notably, the C2 bursts are the only class in which the growth phase is characterized by a direct moisture import through advection $\left(\left\{\vec{v}_h.L_v q\right\} < 0\right)$. After the burst's peak, the DEF becomes positive, which should indicate a decay of the burst. However, rainfall remains relatively constant, but at a much lower precipitation magnitude than in the other two clusters. Another notable difference of the C2 class of bursts is that while the time evolution of moisture advection strongly influences the shape of the time evolution of DEF, its magnitude is much lower than that of the MSE divergence. This indicates that in this class, the WTG assumption does not provide a good approximation for the burst behavior.

The burst classification applied above reveals notable and important differences between the MSE budget of the different burst types identified by it. While C1 follows the "archetypal" MSE and GMS behavior of tropical oceanic convection, C2 and C3 do not. To gain additional insight into the reasons for this behavior, Figure 8 shows maps of the evolution of rainfall and 850 hPa winds through the burst for the three types.

The pre-burst state (Day −3) in C1 is characterized by southeasterly flow in the southeastern half of the analysis area and southwesterly flow in the northwest. Together they form a weak cyclonic circulation centered on the North Australian coastline. By Day 0 the cyclonic circulation strengthens and its center is now located over the Australian Top End. This is accompanied by a large increase in rainfall most visibly over the oceanic and coastal

areas, but also inland. By Day +3 the center of the cyclonic circulation has moved further inland accompanied by a reduction of rainfall over the ocean and coasts. The dominance of oceanic convection in the burst evolution is a possible reason for the likeness of the MSE budget and GMS behavior of this burst type to convection over the tropical oceans reported in earlier studies (Inoue & Back, 2017).

In strong contrast to C1, the bursts in C2 are characterized by easterly and southeasterly flow throughout their evolution. This explains their most frequent occurrence in pre- and post-monsoon conditions. The rainfall pattern on Day 0 shows rainfall maxima over the coastal regions and the Gulf of Carpentaria, but at a significantly lower magnitude than the other burst types. The largely coastal character of the rainfall is consistent with a moistening of a relatively dry pre-/post-monsoon middle troposphere by horizontal advection (see Figure 7n) before the burst to the point where coastal processes can generate local rainfall, while the convection away from the coasts remains suppressed (Bergemann et al., 2015). Narsey et al. (2017) have also shown that bursts early in the season can be strongly affected by extratropical influences, which may well be a key mechanism in rearranging the flow sufficiently to import moisture into our analysis area.

Pre-burst conditions in C3 show widespread easterly to southeasterly flow at Day −3, indicative of the prevalence of these bursts in the post-monsoon season. By Day 0 the rainfall and circulation pattern is very similar to that of the C1 bursts. However, perhaps owing to the seasonal evolution of the monsoon, the cyclonic circulation center is located further north than in C1. While the circulation center moves southwestward by Day +3 as in C1, it remains relatively close to the coast maintaining large rainfall values over the oceanic and coastal regions in the analysis area, thereby leading to a very different evolution of the MSE and GMS than the bursts in C1. An analysis of the International Best Track Archive for Climate Stewardship data set (Knapp et al., 2010) reveals that 13 of the 20 post-monsoon C3 bursts are associated with named Tropical Cyclones, consistent with the evolution of the time evolution of the wind field in Figure 8.

It is interesting to note that the clustering algorithm identified burst types that to first order fall into different phases of the monsoon seasonal cycle. This is likely caused by the strong relationship of the DSE divergence, a variable used in the clustering, and rainfall. As a result, the lighter rainfall events of the pre- and post-monsoon, which occur during quite different synoptic conditions, are identified as their own burst type (C2). Also, as discussed above, the strong and long-lasting bursts (C3) are often associated with tropical cyclones, which tend to occur later in the monsoon seasonal cycle.

The above analysis shows a very close connection of the monsoon burst behavior across the three classes with the synoptic-scale circulation embedded in the even larger-scale monsoon circulation. The differences in both the MSE budget and the GMS evolution are closely associated with the circulation differences. This suggests the need for further investigation of the potential role of the circulation in the MSE budget behavior reported over the open ocean.

4. Summary and Conclusions

This study investigated the evolution of the MSE budget and the GMS for Australian monsoon bursts. There were two main motivations for doing so. First, while the circulation and rainfall behavior of bursts had been studied before (Berry & Reeder, 2016; Narsey et al., 2017), their connection through the energy and moisture budgets had not been clarified. Second, previous work has identified an archetypal cycle in the MSE and GMS for convection over the open ocean. Here we use our ability to define rainfall bursts to extend our knowledge about convective behavior in the tropics to the more complex situation of a mixed land-ocean region affected by the seasonal evolution of a monsoon system.

The main conclusions of our study are:

- *The composite of all monsoon rainfall bursts shows many of the characteristics identified in previous work on oceanic convection*. There is a strong relationship between rainfall and vertically integrated moisture. The evolution of MSE through the burst is dominated by moisture evolution. The evolution of the divergence of MSE is dominated by the horizontal advection of moisture. There is a distinct growth phase of convection before the burst peak, that can be identified by applying the GMS-based concept of DEF. The moistening of the region before the rainfall burst is the result of reduced drying by horizontal advection creating an imbalance that allows the LHF to moisten the region.

- *Despite the many commonalities, the composite of all monsoon bursts also shows major deviations from the behavior of oceanic convection*. The GMS-plane "cycle" of the composite burst does not show a distinct convective decay phase as found over the ocean. This is reflected in all aspects of the MSE budget and GMS, in particular the absence of a positive value of DEF.
- *The differences can be explained through the existence of several distinct types of monsoon bursts as characterized by their GMS evolution*. A cluster analysis of the two components of the GMS reveals three different types of rainfall bursts during the monsoon season. One of these types (C1) behaves similarly to oceanic convection with distinct convective growth and decay phases. This type occurs most frequently during the active monsoon. The other two show very different behaviors. A low-rainfall burst type (C2), mostly found before monsoon onset, is associated with localized coastal convection with little rainfall decay after the burst. A sustained high-rainfall burst type (C3), which occurs mostly near the end or after the retreat of the monsoon, shares its growth characteristics with the typical monsoon burst but shows no decay maintaining very high rainfall levels for at least a week after the burst.
- *Consistent with the large role horizontal moisture advection plays in the MSE budget evolution, the behavior of the different burst types is strongly related to the large-scale monsoon circulation*. The three burst types show distinct circulation characteristics, in particular during and after the rainfall burst. The pre-burst period is dominated by easterly to southeasterly trade wind flow in all three burst types. The weak rainfall bursts (C2) maintain this flow but at a higher level of humidity, allowing coastal rainfall to develop. The decay of rainfall in the "oceanic" monsoon bursts (C1) is associated with a strong southward shift of the cyclonic monsoon circulation away from the coast. In contrast, this circulation is located further north in the burst that maintains rainfall in the region for a long time (C3).

In summary, the application of the MSE budget and GMS concepts to Australian monsoon bursts has broadened our understanding of the physical and dynamical processes involved in their evolution. The objective identification of the bursts has also revealed the different behavior of rainfall in different phases of the Australian monsoon, with low rainfall in the build-up and decay of the monsoon, episodic relatively short bursts in the active monsoon, and strong and long-lasting bursts enhanced by tropical cyclone activity around the termination of the monsoon. The discovery of several distinct types of bursts in our study region raises the question of whether distinct regimes of rainfall behavior also exist over the open ocean and how they might affect the overall MSE and GMS behavior reported in previous studies. The close connection of burst behavior and the larger-scale circulation likely also warrants further investigation of the potential role of the circulation system in oceanic convection.

Appendix A: Mass Flux Correction

Due to the reanalysis output's discrete space and time intervals, as well as the uncertainties in data assimilation, it is not possible to fully close the budgets calculated throughout this study. To reduce budget estimation errors, we first adjusts the wind field to close the column total mass budget before calculating other budgets using the adjusted wind field. The adjustment of column mass is based on the expression:

$$-\frac{1}{g}\frac{\partial p_s}{\partial t} - \nabla \cdot \left\{\rho \vec{v}_h\right\} = P - E. \tag{A1}$$

Where, p_s is the surface pressure and ρ is the density. Equation A1 contains three terms: surface pressure tendency, vertically-integrated mass divergence, and mass gain/loss due to precipitation and evaporation "$P - E$." Applying the divergence theorem to Equation A1 and spatially integrating over an area "A" yields:

$$-\frac{1}{g}\frac{\partial [p_s]}{\partial t} - \frac{1}{A}\oint_{\partial A}\left\{\rho \vec{v}_h\right\} \cdot \vec{n}\, dl = [P] - [E], \tag{A2}$$

where the integral is over the area's boundary, denoted ∂A with a unit normal $\vec{n}$, and the square brackets denote area averages. Incomplete sampling of the inputs to Equation A2 in space and time yields a residual term, "R," equal to the difference between the left and right sides of the equation. Hill et al. (2017) propose adjusting the velocity field at each point along the area boundary to ensure closed mass balance.

$$\vec{v}_{h,adj} = \vec{v}_h - \frac{RAg}{L(p_s - p_{top})}\vec{n}. \tag{A3}$$

Here, $\vec{v}_{h,adj}$ is the adjusted horizontal velocity vector at each level, $\vec{v}_h$ is the original horizontal velocity, and A and L correspond to the area and perimeter of the box, respectively. The adjusted velocity is defined to exactly satisfy Equation A2. We note that the adjustments to the velocity are only defined along the box perimeter and are constant in pressure. Importantly, the adjustments made by this technique are quite small.

Using the adjusted velocity field and the divergence theorem, we may write the MSE budget equation for our analysis area as:

$$\frac{\partial[\{h\}]}{\partial t} + \frac{1}{A}\oint_{\partial A}\left\{h\vec{v}_{h,adj}\right\}\cdot\vec{n}\,dl = L_v[E] + [H] + [R_t] + [R_s]. \tag{A4}$$

So the mass corrected divergence can be written as:

$$\nabla\cdot\left\{h\vec{v}_h\right\} = \frac{1}{A}\oint_{\partial A}\left\{h\vec{v}_{h,adj}\right\}\cdot\vec{n}\,dl = \frac{1}{A}\left(\frac{L_{x1}}{n}\sum_{i=1}^{n}\{h_{Ni}v_{adj,Ni}\} + \frac{L_y}{m}\sum_{i=1}^{m}\{h_{Ei}u_{adj,Ei}\} - \frac{L_y}{m}\sum_{i=1}^{m}\{h_{Wi}u_{adj,Wi}\} - \frac{L_{x2}}{n}\sum_{i=1}^{n}\{h_{Si}v_{adj,Si}\}\right) \tag{A5}$$

Here each sum represents the integral over one of the boundaries. The subscripts N, E, W, and S correspond to the north, east, west, and south boundary of the latitude-longitude box, respectively, $u_{adj,Xi}$ and $v_{adj,Xi}$ are the zonal and meridional wind components at the discrete grid points along each boundary, and m and n are the number of grid points along the boundary in latitude and longitude, respectively. L_{x1} and L_{x2} are the length of northern and southern boundaries, respectively, which depends on the latitude and L_y is the length of the western and eastern boundary.

In a similar procedure, $\nabla\cdot\left\{s\vec{v}_h\right\}$ is calculated.

Data Availability Statement

The ERA5 data for pressure levels and the surface used in this study are available at https://cds.climate.copernicus.eu/cdsapp#!/dataset/reanalysis-era5-pressure-levels?tab=form and https://cds.climate.copernicus.eu/cdsapp#!/dataset/reanalysis-era5-single-levels?tab=form.DatafromtheMERRA-2 can be found at https://disc.gsfc.nasa.gov/datasets?project=MERRA-2. Data from the Global Precipitation Climatology Project can be found at http://apdrc.soest.hawaii.edu/las/v6/dataset?catitem=12802. Python was used to create all of the figures.

Acknowledgments
This research was funded by the Australian Research Council's (ARC) Centre of Excellence for Climate Extremes (CE170100023) and the ARC Discovery Project (DP200102954). S.M. was supported by a scholarship from the Australian Government's Research Training Program. The Australian government-supported National Computational Infrastructure provided computing resources. As part of the Wiley-Monash University agreement, which was facilitated by the Council of Australian University Librarians, Monash University facilitated open-access publishing. Open access publishing facilitated by Monash University, as part of the Wiley - Monash University agreement via the Council of Australian University Librarians.

References

Adeloye, A. J., & Rustum, R. (2011). Lagos (Nigeria) flooding and influence of urban planning. *Proceedings of the Institution of Civil Engineers-Urban Design and Planning*, *164*(3), 175–187. https://doi.org/10.1680/udap.1000014

Adler, R., Wang, J., Sapiano, M., Huffman, G., Bolvin, D., & Nelkin, E. (2022). *Program, 2017: Global precipitation climatology project (GPCP) climate data record (CDR), version 1.3 (daily)*. NOAA National Centers for Environmental Information.

Baraldi, A., & Blonda, P. (1999). A survey of fuzzy clustering algorithms for pattern recognition. I. *IEEE Transactions on Systems, Man, and Cybernetics, Part B (Cybernetics)*, *29*(6), 778–785. https://doi.org/10.1109/3477.809032

Benedict, J. J., Maloney, E. D., Sobel, A. H., & Frierson, D. M. (2014). Gross moist stability and MJO simulation skill in three full-physics GCMS. *Journal of the Atmospheric Sciences*, *71*(9), 3327–3349. https://doi.org/10.1175/jas-d-13-0240.1

Bergemann, M., Jakob, C., & Lane, T. P. (2015). Global detection and analysis of coastline-associated rainfall using an objective pattern recognition technique. *Journal of Climate*, *28*(18), 7225–7236. https://doi.org/10.1175/jcli-d-15-0098.1

Berry, G. J., & Reeder, M. J. (2016). The dynamics of Australian monsoon bursts. *Journal of the Atmospheric Sciences*, *73*(1), 55–69. https://doi.org/10.1175/JAS-D-15-0071.1

Berry, G. J., Reeder, M. J., & Jakob, C. (2012). Coherent synoptic disturbances in the Australian monsoon. *Journal of Climate*, *25*(24), 8409–8421. https://doi.org/10.1175/JCLI-D-12-00143.1

Bretherton, C. S., Peters, M. E., & Back, L. E. (2004). Relationships between water vapor path and precipitation over the tropical oceans. *Journal of Climate*, *17*(7), 1517–1528. https://doi.org/10.1175/1520-0442(2004)017<1517:rbwvpa>2.0.co;2

Chou, C., Neelin, J. D., Chen, C.-A., & Tu, J.-Y. (2009). Evaluating the "rich-get-richer" mechanism in tropical precipitation change under global warming. *Journal of Climate*, *22*(8), 1982–2005. https://doi.org/10.1175/2008jcli2471.1

Davidson, N. E., Tory, K. J., Reeder, M. J., & Drosdowsky, W. L. (2007). Extratropical–tropical interaction during onset of the Australian monsoon: Reanalysis diagnostics and idealized dry simulations. *Journal of the Atmospheric Sciences*, *64*(10), 3475–3498. https://doi.org/10.1175/jas4034.1

Drosdowsky, W. (1996). Variability of the Australian summer monsoon at Darwin: 1957–1992. *Journal of Climate*, *9*(1), 85–96. https://doi.org/10.1175/1520-0442(1996)009<0085:votasm>2.0.co;2

Evans, S., Marchand, R., & Ackerman, T. (2014). Variability of the Australian monsoon and precipitation trends at Darwin. *Journal of Climate*, *27*(22), 8487–8500. https://doi.org/10.1175/jcli-d-13-00422.1

Evans, S., Marchand, R., Ackerman, T., & Beagley, N. (2012). Identification and analysis of atmospheric states and associated cloud properties for Darwin, Australia. *Journal of Geophysical Research*, *117*(D6). https://doi.org/10.1029/2011jd017010

Frei, C., Davies, H. C., Gurtz, J., & Schär, C. (2000). Climate dynamics and extreme precipitation and flood events in central Europe. *Integrated Assessment*, *1*(4), 281–300. https://doi.org/10.1023/a:1018983226334

Gadgil, S. (2018). The monsoon system: Land–sea breeze or the itcz? *Journal of Earth System Science*, *127*(1), 1–29. https://doi.org/10.1007/s12040-017-0916-x

Gelaro, R., McCarty, W., Suárez, M. J., Todling, R., Molod, A., Takacs, L., et al. (2017). The modern-era retrospective analysis for research and applications, version 2 (MERRA-2). *Journal of Climate*, *30*(14), 5419–5454. https://doi.org/10.1175/jcli-d-16-0758.1

Gentleman, R., & Carey, V. J. (2008). Unsupervised machine learning. In *Bioconductor case studies* (pp. 137–157). Springer.

Hannah, W. M., & Maloney, E. D. (2011). The role of moisture–convection feedbacks in simulating the Madden–Julian oscillation. *Journal of Climate*, *24*(11), 2754–2770. https://doi.org/10.1175/2011jcli3803.1

Hendon, H. H., & Liebmann, B. (1990). The intraseasonal (30–50 day) oscillation of the Australian summer monsoon. *Journal of the Atmospheric Sciences*, *47*(24), 2909–2924. https://doi.org/10.1175/1520-0469(1990)047⟨2909:TIDOOT⟩2.0.CO;2

Hill, S. A., Ming, Y., Held, I. M., & Zhao, M. (2017). A moist static energy budget–based analysis of the Sahel rainfall response to uniform oceanic warming. *Journal of Climate*, *30*(15), 5637–5660. https://doi.org/10.1175/JCLI-D-16-0785.1

Hill, S. A., Ming, Y., & Zhao, M. (2018). Robust responses of the Sahelian hydrological cycle to global warming. *Journal of Climate*, *31*(24), 9793–9814. https://doi.org/10.1175/JCLI-D-18-0238.1

Holloway, C. E., & Neelin, J. D. (2009). Moisture vertical structure, column water vapor, and tropical deep convection. *Journal of the Atmospheric Sciences*, *66*(6), 1665–1683. https://doi.org/10.1175/2008jas2806.1

Inoue, K., & Back, L. E. (2015). Gross moist stability assessment during TOGA COARE: Various interpretations of gross moist stability. *Journal of the Atmospheric Sciences*, *72*(11), 4148–4166. https://doi.org/10.1175/JAS-D-15-0092.1

Inoue, K., & Back, L. E. (2017). Gross moist stability analysis: Assessment of satellite-based products in the GMS plane. *Journal of the Atmospheric Sciences*, *74*(6), 1819–1837. https://doi.org/10.1175/JAS-D-16-0218.1

Inoue, K., Biasutti, M., & Fridlind, A. M. (2021). Evidence that horizontal moisture advection regulates the ubiquitous amplification of rainfall variability over tropical oceans. *Journal of the Atmospheric Sciences*, *78*(2), 529–547. https://doi.org/10.1175/JAS-D-20-0201.1

Kajikawa, Y., Wang, B., & Yang, J. (2010). A multi-time scale Australian monsoon index. *International Journal of Climatology*, *30*(8), 1114–1120. https://doi.org/10.1002/joc.1955

Keenan, T. D., & Brody, L. R. (1988). Synoptic-scale modulation of convection during the Australian summer monsoon. *Monthly Weather Review*, *116*(1), 71–85. https://doi.org/10.1175/1520-0493(1988)116⟨0071:SSMOCD⟩2.0.CO;2

Knapp, K. R., Kruk, M. C., Levinson, D. H., Diamond, H. J., & Neumann, C. J. (2010). The international best track archive for climate stewardship (IBTrACS) unifying tropical cyclone data. *Bulletin of the American Meteorological Society*, *91*(3), 363–376. https://doi.org/10.1175/2009bams2755.1

Krishnamurti, T. N., & Chang, C.-P. (1987). *Monsoon meteorology*. Oxford University Press.

Lloyd, S. (1982). Least squares quantization in PCM. *IEEE Transactions on Information Theory*, *28*(2), 129–137. https://doi.org/10.1109/tit.1982.1056489

McBride, J. L., & Frank, W. M. (1999). Relationships between stability and monsoon convection. *Journal of the Atmospheric Sciences*, *56*(1), 24–36. https://doi.org/10.1175/1520-0469(1999)056<0024:rbsamc>2.0.co;2

Moise, A., Smith, I., Brown, J. R., Colman, R., & Narsey, S. (2020). Observed and projected intra-seasonal variability of Australian monsoon rainfall. *International Journal of Climatology*, *40*(4), 2310–2327. https://doi.org/10.1002/joc.6334

Narsey, S., Reeder, M. J., Ackerley, D., & Jakob, C. (2017). A midlatitude influence on Australian monsoon bursts. *Journal of Climate*, *30*(14), 5377–5393. https://doi.org/10.1175/JCLI-D-16-0686.1

Neelin, J., & Held, I. (1987). Modeling tropical convergence based on the moist static energy budget. *Monthly Weather Review*, *115*(1), 3–12. https://doi.org/10.1175/1520-0493(1987)115⟨0003:MTCBOT⟩2.0.CO;2

Nicholls, N., McBride, J., & Ormerod, R. (1981). *On predicting the onset of the Australian wet-season at Darwin*. Australian Numerical Meteorology Research Centre.

Pope, M., Jakob, C., & Reeder, M. J. (2008). Convective systems of the north Australian monsoon. *Journal of Climate*, *21*(19), 5091–5112. https://doi.org/10.1175/2008jcli2304.1

Pope, M., Jakob, C., & Reeder, M. J. (2009). Regimes of the north Australian wet season. *Journal of Climate*, *22*(24), 6699–6715. https://doi.org/10.1175/2009jcli3057.1

Raymond, D. J., & Fuchs, Ž. (2007). Convectively coupled gravity and moisture modes in a simple atmospheric model. *Tellus A: Dynamic Meteorology and Oceanography*, *59*(5), 627–640. https://doi.org/10.1111/j.1600-0870.2007.00268.x

Raymond, D. J., Sessions, S. L., Sobel, A. H., & Fuchs, Ž. (2009). The mechanics of gross moist stability. *Journal of Advances in Modeling Earth Systems*, *1*(3). https://doi.org/10.3894/JAMES.2009.1.9

Rossow, W. B., Tselioudis, G., Polak, A., & Jakob, C. (2005). Tropical climate described as a distribution of weather states indicated by distinct mesoscale cloud property mixtures. *Geophysical Research Letters*, *32*(21). https://doi.org/10.1029/2005gl024584

Sekizawa, S., Nakamura, H., & Kosaka, Y. (2023). Interannual variability of the Australian summer monsoon sustained through internal processes: Wind–evaporation feedback, dynamical air–sea interaction, and soil moisture memory. *Journal of Climate*, *36*(3), 983–1000. https://doi.org/10.1175/jcli-d-22-0116.1

Slingo, A., & Slingo, J. (1988). The response of a general circulation model to cloud longwave radiative forcing. I: Introduction and initial experiments. *Quarterly Journal of the Royal Meteorological Society*, *114*(482), 1027–1062. https://doi.org/10.1002/qj.49711448209

Sobel, A. H., Nilsson, J., & Polvani, L. M. (2001). The weak temperature gradient approximation and balanced tropical moisture waves. *Journal of the Atmospheric Sciences*, *58*(23), 3650–3665. https://doi.org/10.1175/1520-0469(2001)058<3650:twtgaa>2.0.co;2

Tonidandel, S., & LeBreton, J. M. (2011). Relative importance analysis: A useful supplement to regression analysis. *Journal of Business and Psychology*, *26*(1), 1–9. https://doi.org/10.1007/s10869-010-9204-3

Troup, A. (1961). Variations in upper tropospheric flow associated with the onset of the Australian summer monsoon. *MAUSAM*, *12*(2), 217–230. https://doi.org/10.54302/mausam.v12i2.4184

Wang, B. (2006). *The Asian monsoon*. Springer Science & Business Media. https://doi.org/10.1007/3-540-37722-0